

Article

Hydropyrolysis of *n*-Hexane and Toluene to Acetylene in Rotating-Arc Plasma

Jie Ma, Ming Zhang, Jianhua Wu, Qiwei Yang * , Guangdong Wen, Baogen Su * and Qilong Ren

Key Laboratory of Biomass Chemical Engineering of Ministry of Education, Department of Chemical and Biological Engineering, Zhejiang University, Hangzhou 310027, China; 11028061@zju.edu.cn (J.M.); phoenix0227@zju.edu.cn (M.Z.); mace@zju.edu.cn (J.W.); zdwgd@zju.edu.cn (G.W.); renql@zju.edu.cn (Q.R.)

* Correspondence: yangqw@zju.edu.cn (Q.Y.); subg@zju.edu.cn (B.S.);

Tel.: +86-571-8795-1125 (Q.Y.); +86-571-8795-1125 (B.S.)

Received: 30 March 2017; Accepted: 28 June 2017; Published: 1 July 2017

Abstract: Thermal plasma pyrolysis is a powerful technology for converting waste or low-value materials to valuable gaseous hydrocarbons. This paper presents for the first time the hydropyrolysis of *n*-hexane and toluene in a rotating-arc plasma reactor. Effects of the mole ratio of H/C in the feed, power input and magnetic induction were investigated to evaluate the reaction performance. A lower H/C ratio could lead to a lower yield of C₂H₂ and lower specific energy consumption, and there existed an optimum range of power input for both *n*-hexane and toluene pyrolysis within the investigated range. The yield of C₂H₂ in *n*-hexane and toluene pyrolysis could reach 85% and 68%, respectively, with respective specific energy consumption (SEC) of 13.8 kWh/kg·C₂H₂ and 19.9 kWh/kg·C₂H₂. Compared with the results reported in literature, the rotating-arc plasma process showed higher C₂H₂ yield and lower energy consumption, which is attributed to the better initial mixing of the reactant with the hot plasma gas and the more uniform temperature distribution.

Keywords: thermal plasma; hydropyrolysis; hexane; toluene; acetylene

1. Introduction

The plasma process has emerged as an innovative way to convert various carbonaceous materials to valuable chemicals [1]. The materials vary diversely, including gaseous hydrocarbon [2–4], liquid hydrocarbon [5,6], coal [7,8], polymer [9,10], biomass [11,12] and solid waste [13,14], etc., and the target products differ from syngas to valuable chemicals such as acetylene, ethylene and carbon nanotube.

The plasma could be classified as non-thermal plasma (cold plasma) and thermal plasma. The non-thermal plasma has the nature of non-equilibrium in the electron and the heavy particle temperature [15], which is beneficial for the initiation of chemical reaction under relatively lower temperature and energy input [4,16]. However, the chemical process usually suffers from lower conversion efficiency and lower throughput in non-thermal plasma reactor. The thermal plasma [17,18] has a similar temperature for both the electron and the heavy particle, and is characterized with high enthalpy density, high chemical reactivity and high throughput, which provides a viable way for the thermal chemical process [19,20].

Acetylene is one important raw material for the production of polyvinyl chloride (PVC), butanediol, acetaldehyde and so on [21]. The traditional partial oxidation (POX) process to produce acetylene suffers from lower acetylene selectivity due to the introduction of oxygen [22]. The thermal plasma technology has been applied for the highly endothermic process of acetylene production [3,7,23,24]. Since the process is carried out in the non-oxidative medium with abundant free radicals and high temperature, the C₂H₂ selectivity is much higher than the POX process, and the conversion of feedstock and yield of gases could be higher than conventional non-plasma pyrolysis.

Furthermore, the plasma pyrolysis is an ultra-fast process with the scale of milliseconds. Chen et al. [25] investigated the pyrolysis of liquefied petroleum gas (LPG) in H_2/Ar plasma, and the conversion of LPG achieved 76% with C_2H_2 yield of 74%. Yan et al. [6] investigated the pyrolysis of some liquid hydrocarbons in H_2/Ar plasma. Beiers et al. [26] investigated the pyrolysis of some gaseous and liquid hydrocarbons in hydrogen plasma, such as cyclohexane, benzene, toluene, coal oil and anthracite oil.

Generally, the thermal plasma reaction processes were carried out in a two-stage reactor, which contains a plasma generator section and a reaction section, and the reactant is fed below the hot plasma jet. However, the thermal plasma conversion of chemicals in those reactors usually suffers from poor mixing efficiency between the reactants and the hot plasmas, which is attributed to the inhomogeneous feature of the plasma jet and the thermal resistant effect [27].

To address the issue, the rotating-arc plasma driven by the Lorentz force in an external magnetic field is one promising way [28–30]. The intensified flow turbulence caused by rotating will improve the uniformity of plasma, and the feeding of reactant above the plasma jet in such reactor will enhance the mixing of reactant with hot plasma. Both of these are beneficial for the chemical reaction, and have been applied in the pyrolysis of gaseous hydrocarbons, glycerol and coal to produce acetylene or syngas [12,31].

Herein, we for the first time report the pyrolysis of *n*-hexane and toluene to acetylene in rotating-arc plasma. The straight-chain *n*-hexane and aromatic toluene are chosen to gain insights into the pyrolysis of liquid hydrocarbons. The feed was injected upstream the plasma jet, allowing better initial mixing efficiency between the reactants and the hot plasma gas. The effect of key parameters such as the mole ratio of H/C in feed ($R_{H/C}$), the power input (P) and the magnetic induction intensity (B) on reaction performance was demonstrated, and the comparison of C_2H_2 production efficiency was carried out between this work and the reference studies. Hydrogen gas was input into the reactor as the plasma working medium. Hydrogen molecular (H_2) will dissociate to hydrogen radical ($H\cdot$), which will react with liquid hydrocarbons and intermediates to promote the pyrolysis process. Moreover, the decomposition of acetylene to soot will be suppressed with the presence of hydrogen.

2. Experimental and Methods

2.1. Materials

The *n*-hexane (Analytical Reagent, AR) and the toluene (AR) were obtained from the Sinopharm Group Co. Ltd. (Shanghai, China). Both the liquid hydrocarbon and the plasma gas were introduced into the reactor through the annular gap (2.0 mm) between the cathode and the reactor.

2.2. Pyrolysis Experiment

The plasma pyrolysis system consists of three parts: a direct current (DC) power supply, a rotating-arc plasma reactor and a sampling/analysis system. The plasma was generated with a DC power source with maximum capacity of 50 kW, and equipped with a rod-type tungsten cathode with a diameter of 6.0 mm, a water-cooled copper anode with an internal diameter of 25.0 mm with an exciting coil (Figure 1). A water cooling section is placed at the outlet of the plasma reactor, which is used to prevent the degradation of the produced acetylene. All the experiments were carried at the atmospheric pressure. Experiment was carried out for three times, and the error was within 12.0%. The error was relatively high due to the extreme reaction conditions (e.g., high temperature, strong turbulence) inside the plasma reactor.

The products gas was sampled by two gas chromatographs, Shimadzu GC-2010 Plus (Shimadzu Co., Ltd., Kyoto, Japan) and Kexiao GC-1690 (Hangzhou Kexiao Chemical Equipment Co., Ltd., Hangzhou, China). The concentrations of gaseous hydrocarbons such as CH_4 , C_2H_2 and C_2H_4 were determined by hydrogen flame ionization detector (FID) with a HP-AL/S capillary column (Agilent Technologies Co., Ltd., Santa Clara, CA, USA); Ar and H_2 were determined by thermal

conductivity detector with a PLOT 5A packed column (Agilent Technologies Co., Ltd., Santa Clara, CA, USA).

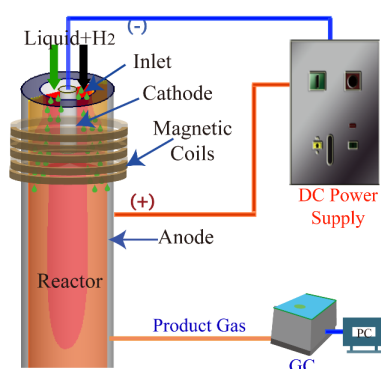


Figure 1. Schematic view of the rotating-arc plasma reactor.

To evaluate the reaction performance, the carbon-based yield (Y) of C_2H_2 is defined as:

$$Y_{C_2H_2} = \frac{2 \times \frac{m_{C_2H_2}}{26}}{x \times \frac{m_{C_xH_y}}{M_{C_xH_y}}} \times 100\% \quad (1)$$

where m is the mass flow rate, and C_xH_y represents the feed formula and M is molecular weight.

The specific energy consumption (SEC) expressing the economic value of this process is defined as:

$$SEC \text{ (kWh/kg} \cdot C_2H_2) = \frac{\text{Input power (kW)}}{\text{Mass flow rate of } C_2H_2 \text{ (kg/h)}} \quad (2)$$

2.3. Numerical Simulation

Thermodynamic simulation was carried out with the minimum Gibbs energy method [32]. A representative ratio of H/C was set at 6.0, with the equilibrium temperature varying from 500 to 4500 K.

Kinetic simulation was carried out with a plug flow reactor (PFR) model, with the assumption that the liquid feed is instantaneously vaporized due to the high temperature in the plasma reactor. The JetSurF V2.0 mechanism [33] and the USC Mech V2.0 mechanism [34] are used to simulate the hexane pyrolysis, and the Zhang mechanism [35] is used to simulate the toluene pyrolysis. The equilibrium model and the PFR model in the CHEMKIN software are used to investigate the thermodynamic and kinetic analysis, respectively.

3. Results and Discussion

3.1. Effect of Mole Ratio of H/C

In this section, the flow rate of H_2 was $5.0 \text{ Nm}^3/\text{h}$, the arc current was 80 A with a power input of 14.5 kW and magnetic induction of 0.058 T. The mole ratio of H/C was adjusted by varying the feeding rate of *n*-hexane (15.0–42.0 g/min) or toluene (10.0–25.0 g/min). As observed in Figure 2a,b, under all the conditions, the concentration of C_2H_2 was always much higher than those of C_2H_4 and CH_4 , suggesting that C_2H_2 can be obtained as the main product from the pyrolysis of both aliphatic *n*-hexane and aromatic toluene in the rotating-arc plasma.

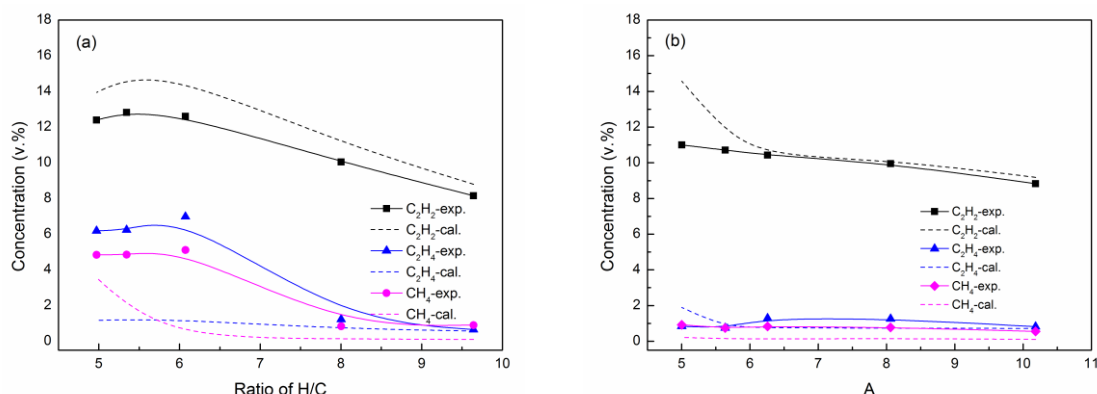


Figure 2. The effect of H/C mole ratio on the concentration of C_2H_2 , C_2H_4 and CH_4 in the pyrolysis product of *n*-hexane (a) and toluene (b), exp.: experimental data, cal.: calculated kinetic data. Reaction conditions: $Q_{H_2} = 5.0 \text{ Nm}^3/\text{h}$, $I = 80 \text{ A}$, $P = 14.5 \text{ kW}$, $B = 0.058 \text{ T}$, *m-n*-hexane = 15.0–42.0 g/min, *m*-toluene = 10.0–25.0 g/min.

With the increase of H/C ratio (decrease of the hydrocarbon feed rate), the concentration of all the products of *n*-hexane pyrolysis increased slightly at the beginning ($H/C < 6.0$, Figure 2a), which is attributed to the higher energy input per mass feed. Then the gas concentrations decreased gradually, especially for the C_2H_4 and CH_4 concentration. The experimental C_2H_2 mole fraction shows a similar trend with the kinetic data with increasing the H/C ratio. However, the C_2H_4 mole fraction is much higher than the kinetic result especially at lower H/C ratio, which is attributed to the relatively lower reaction temperature. As for the toluene pyrolysis (Figure 2b), the C_2H_2 concentration decreased monotonically, while both the C_2H_4 and CH_4 concentration almost kept steady within the operating range. The experimental data also show similar trend with the kinetic data for the toluene pyrolysis.

According to the kinetic analysis, with increasing the H/C ratio, the system temperature varies from 1720 to 2800 K. As shown in Figure 3, the C_2H_2 was the predominant hydrocarbon product over a wide range of 1700–3500 K in the equilibrium system, which is consistent with the kinetic simulation results. However, the simulated equilibrium C_2H_4 concentration was lower than the CH_4 concentration, which is different with the experimental result (Figures 2 and 3). It indicates that the product distribution of pyrolysis is kinetically controlled, which is similar to the results of references [26]. Ethylene is the major intermediate for the formation of acetylene [36,37], and lower temperature is favorable for the production of ethylene. In fact, the pyrolysis reaction only takes milliseconds, thus the pyrolysis performance should be significantly influenced by the volatilization efficiency of liquid feedstock.

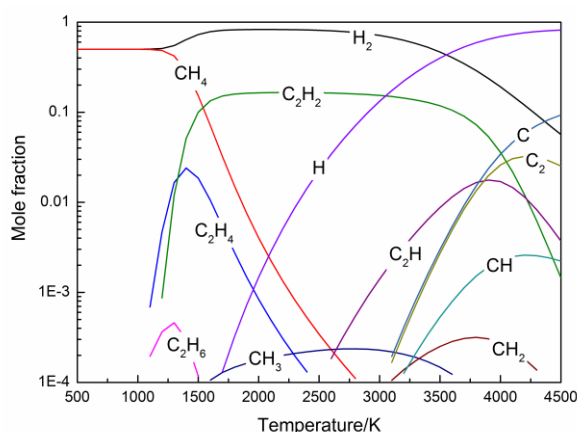


Figure 3. The equilibrium composition of H-C system ($H/C = 6.0$).

Since high temperature is beneficial for the conversion of the feed and the production of C_2H_2 , the C_2H_2 yield increased for both the *n*-hexane and toluene pyrolysis with the increase of H/C ratio (Figure 4). Although the conversion efficiency of hydrocarbon should be improved with a decreasing feed rate due to the rising energy input per mass feed, the specific energy consumption (SEC) of C_2H_2 increased because the total C_2H_2 amount decreased with lower hydrocarbon feed rate (higher H/C ratio). Attributed to the high sooting tendency of the aromatic compound [38,39], the *n*-hexane showed a lower SEC than the toluene, which is consistent with the results that the straight-chain hydrocarbon shows lower energy consumption for acetylene production than the aromatic hydrocarbon [6,25].

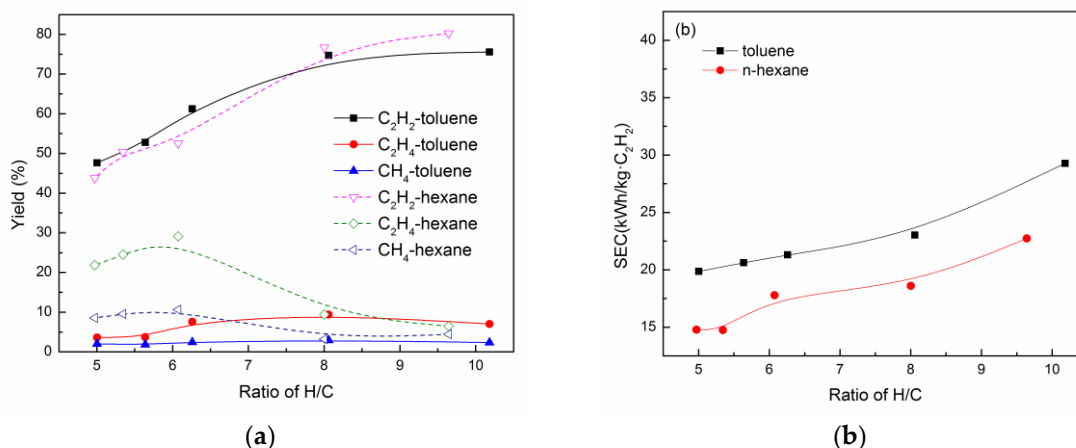


Figure 4. (a) The effect of H/C mole ratio on the yield, and (b) SEC of C_2H_2 . Reaction conditions: $Q_{H_2} = 5.0 \text{ Nm}^3/\text{h}$, $I = 80 \text{ A}$, $P = 14.5 \text{ kW}$, $B = 0.058 \text{ T}$, *m-n*-hexane = 15.0–42.0 g/min, *m*-toluene = 10.0–25.0 g/min.

3.2. Effect of Power Input

In this section, the H/C mole ratio was fixed at 6.5 for both *n*-hexane and toluene with a magnetic induction of $B = 0.058 \text{ T}$. The arc currents are 60–200 A (*n*-hexane) and 60–180 A (toluene) with an interval of 20 A. As shown in Figure 5, the concentration of C_2H_2 had a peak point with the increase of power input in both *n*-hexane and toluene pyrolysis process. On the contrary, the concentrations of CH_4 and C_2H_4 decreased with the increase in the power input from 9.3 to 14.2 kW, and then increase slowly when the value is higher than 14.2 kW in the *n*-hexane pyrolysis process. As for the toluene pyrolysis, the concentrations of CH_4 and C_2H_4 fluctuated in a low concentration range with no significant changes. Generally, higher energy input is favorable for the formation of C_2H_2 because it requires high temperature. However, excessive energy input will lead to higher C_2H_2 degradation rate due to an over-high temperature. Therefore, an optimum specific energy input range is available for the pyrolysis of hydrocarbons according to the feed rate. This is consistent with the thermodynamic simulation results in Figure 3, in which an optimum temperature range could be found.

The yield of C_2H_2 in the *n*-hexane pyrolysis increased with the increasing power input from 9.3 to 13.6 kW, and then decreased with further increase of power input, showing a maximum yield of 83.50% at 13.6 kW (Figure 6a). Comparably, the yield of C_2H_2 shows a similar trend with the increase of power input in the toluene pyrolysis, with a maximum yield of 68.64% at 16.4 kW. This trend is ascribed again to the fact that excessive power input would increase the degradation rate of C_2H_2 . The reason why the C_2H_2 yield from *n*-hexane was much higher than that from toluene is because more energy is needed for the pyrolysis of toluene to reach the maximum yield of C_2H_2 . This is attributed to the difference in bond dissociation energy (BDE), where the BDE of C–C bond in toluene ($\sim 426.8 \text{ kJ/mol}$) is larger than that in *n*-hexane ($\sim 363.6 \text{ kJ/mol}$), and the BDE of C–H in the aromatics (465–478 kJ/mol) is also larger than that in the straight-chain alkanes ($\sim 410 \text{ kJ/mol}$) [40]. Therefore, the *n*-hexane showed lower SEC than toluene under the same power input range (Figure 6b), which is attributed to the fact

the aromatic substance has high sooting tendency [41]. The minimum SEC that could be achieved was 21.1 kWh/kg·C₂H₂ for toluene, and 13.5 kWh/kg·C₂H₂ for *n*-hexane, respectively.

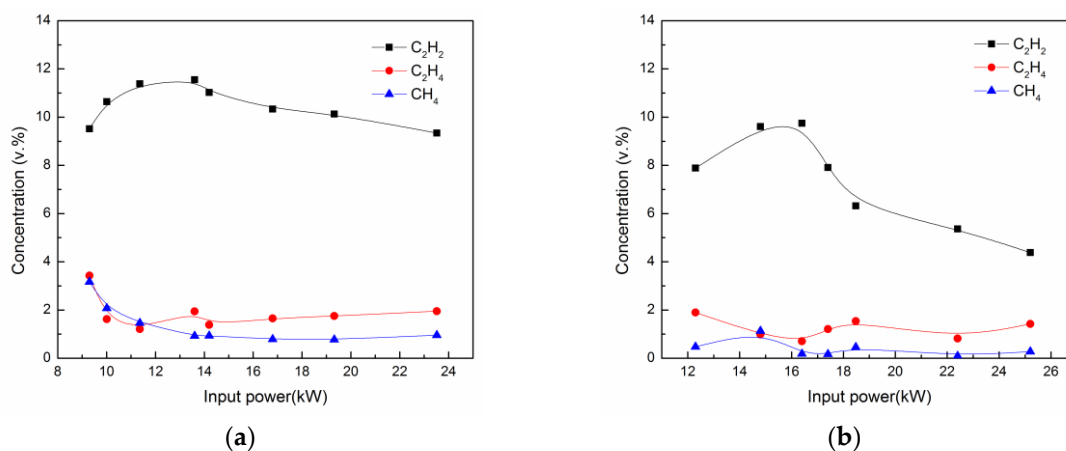


Figure 5. The effect of power input on the concentration of C₂H₂, C₂H₄ and CH₄ in the pyrolysis product of *n*-hexane (a) and toluene (b). Reaction conditions: (a) R_{H/C} = 6.5, Q_{H₂} = 4.0 Nm³/h, *m-n*-hexane = 20.5 g/min, B = 0.058 T, P = 9.3–23.5 Kw; (b) R_{H/C} = 6.5, Q_{H₂} = 5.0 Nm³/h, *m*-toluene = 18.8 g/min, P = 12.3–25.2 kW, B = 0.058 T.

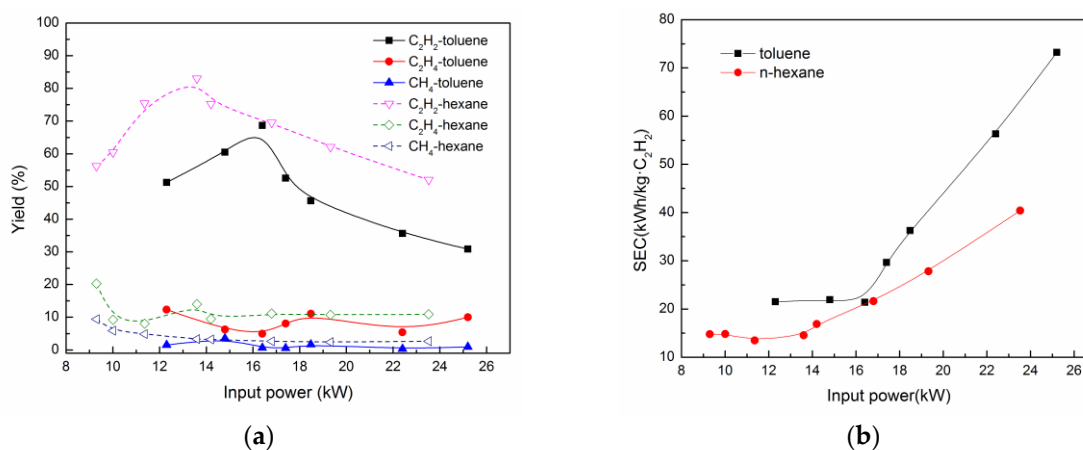


Figure 6. The effect of power input on the yield (a) and specific energy consumption (SEC) (b) of C₂H₂. Reaction conditions: (a) R_{H/C} = 6.5, Q_{H₂} = 4.0 Nm³/h, *m-n*-hexane = 20.5 g/min, B = 0.058 T, P = 9.3–23.5 kW; (b) R_{H/C} = 6.5, Q_{H₂} = 5.0 Nm³/h, *m*-toluene = 18.8 g/min, P = 12.3–25.2 kW, B = 0.058 T.

3.3. Effect of Magnetic Induction

In this section, the effect of magnetic induction with value varying from 0.02–0.10 T was investigated. As shown in Figure 7, within the investigated range the magnetic induction has no significant effect on the composition of pyrolysis gas and the yield of C₂H₂ in the *n*-hexane pyrolysis. However, the SEC of C₂H₂ in the pyrolysis of *n*-hexane decreased with the increase of magnetic induction. The effect of magnetic induction on the pyrolysis of toluene was more significant. As illustrated in Figure 8, both the concentration and the yield of C₂H₂ increased sharply with the increasing of magnetic induction from 0.02 to 0.077 T, and then decreased with a larger magnetic induction. Higher magnetic induction means higher rotational speed of plasma arc due to a stronger Lorentz force. Since the feed is injected upstream the plasma, the intensified turbulence is not only beneficial for the initial mixing between the reactants and the hot plasma gas, but also will create a more uniform distribution of temperature within the reactor. Therefore, the conversion efficiency will

be improved at the beginning of increasing magnetic induction, especially for the toluene pyrolysis process. On the other hand, the feed will move fast toward the cooling wall direction with stronger centrifugal force caused by larger magnetic induction. Due to the different tendency of soot formation, the soot formation rate accelerated for the toluene pyrolysis process, resulting in the decrease of the yield of C_2H_2 at over-high magnetic induction. Whereas, with a lower soot formation ability of *n*-hexane, the *n*-hexane pyrolysis performance was not significantly affected by the centrifugal effect.

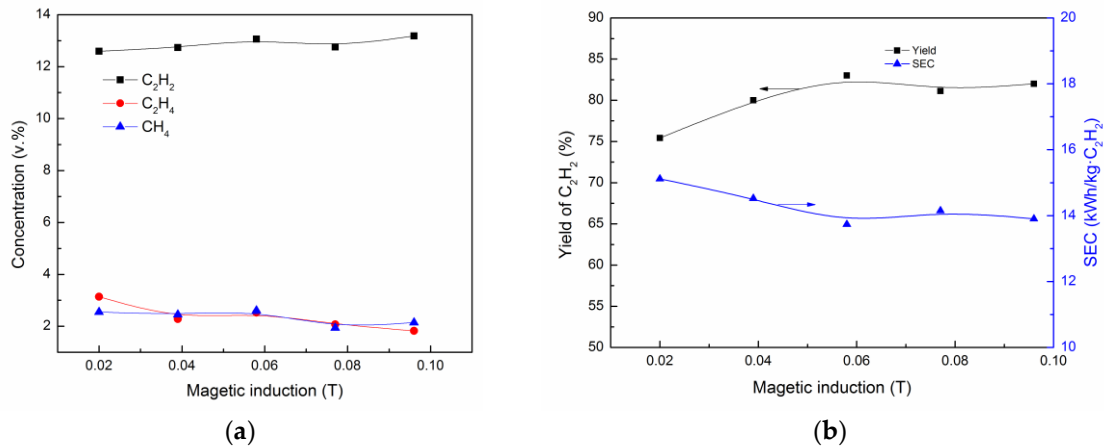


Figure 7. The effect of magnetic induction on the performance of *n*-hexane pyrolysis: (a) concentration in product gas; (b) C_2H_2 yield and SEC. Reaction conditions: $R_{H/C} = 6.3$, $Q_{H_2} = 5.0 \text{ Nm}^3/\text{h}$, *m-n*-hexane = 27.4 g/min, $B = 0.02\text{--}0.10 \text{ T}$, $I = 80 \text{ A}$, $P = 17.0 \text{ kW}$.

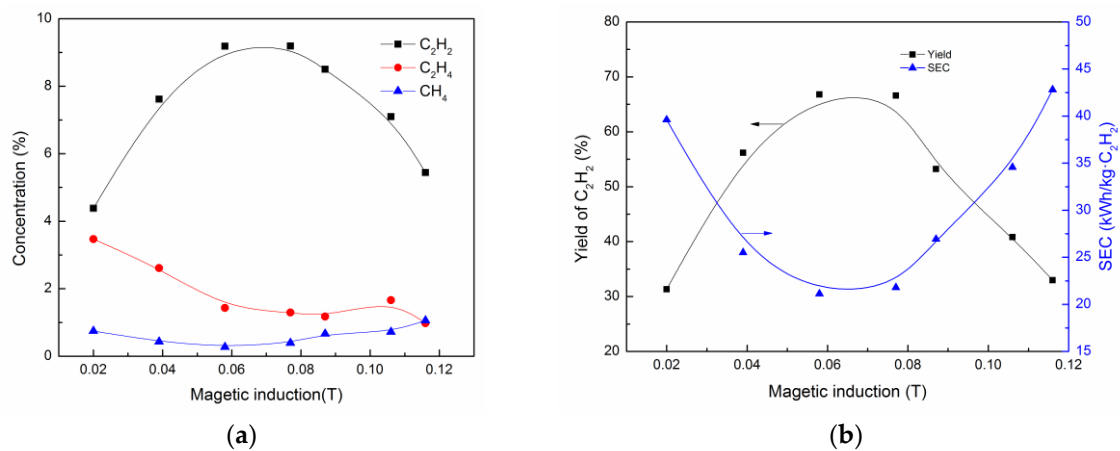


Figure 8. The effect of magnetic induction on the performance of toluene pyrolysis. (a) concentration, (b) yield and SEC; Reaction conditions: toluene, $Q_{H_2} = 5.0 \text{ Nm}^3/\text{h}$, *m*-toluene = 18.8 g/min, $B = 0.02\text{--}0.10 \text{ T}$, $I = 80 \text{ A}$, $P = 16.0 \text{ kW}$.

The rotational speed of plasma arc could be expressed as follows [42]:

$$v = 78I^{4/9}B^{0.6}\rho_0^{-8/9}\varphi^{-1/3} \quad (3)$$

where v is the arc velocity, I is the arc current, B is the magnetic induction, ρ is gas density, φ can be represented by the axial gas velocity v_a as follows:

$$\varphi = \frac{1}{1 + v_a} + v_a \quad (4)$$

Taking the $B = 0.058$ T for example, the calculated rotating velocity is 218 m/s, which is around 2775 r/s.

3.4. Comparison with Different Plasma Processes

Table 1 shows the operation conditions and performance of liquid hydrocarbons pyrolysis process reported in literatures (traditional linear-type plasma reactor) and current work (rotating plasma reactor). It is observed that the rotating-arc plasma reactor in the current work shows higher yield of C_2H_2 and lower SEC for both the *n*-hexane and the toluene pyrolysis process. The lower SEC in this work is attributed to the improved mixing efficiency and enlarged high-temperature zone by the rotating-arc. For instance, even with a lower specific energy input (3.84×10^4 kJ/kg) in case 1 of the current work, the yield of C_2H_2 is up to 83.01% and SEC of 13.73 kWh/kg C_2H_2 , whereas the yield of C_2H_2 is 70.00% and SEC of 18.00 kWh/kg C_2H_2 in case 6 of reference with a higher energy input (4.70×10^4 kJ/kg). This could be attributed to the intensified turbulence caused by rotating arc that will improve the initial mixing of reactants with hot plasma gas and improve the temperature homogenization.

Table 1. Typical operating conditions and performance of liquid hydrocarbons pyrolysis process.

	Unit	This Work				Ref. [6]		Ref. [25]		
Num.		1	2	3	4	5	6	7	8	9
Feedstock	-	<i>n</i> -hexane	<i>n</i> -hexane	toluene	toluene	<i>n</i> -hexane	<i>n</i> -hexane	toluene	<i>n</i> -hexane	toluene
Feed rate	g/min	27.40	20.54	18.81	18.81	3.30	2.55	2.60	40	40
Input power	kW	17.52	13.60	16.40	15.75	3.3	2.0	2.28	23.08	30.34
Specific input power	kJ/kg	3.84×10^4	3.97×10^4	5.23×10^4	5.03×10^4	6.01×10^4	4.70×10^4	5.26×10^4	1.04×10^5	7.91×10^4
C ₂ H ₂	v/v %	13.06	11.55	9.75	9.19	5.89	11.95	2.27	3.60	3.83
CH ₄	v/v %	3.42	0.93	0.18	0.27	2.83	2.33	0.77	0.65	0.23
C ₂ H ₄	v/v %	2.43	1.95	0.71	1.43	4.40	2.85	0.09	0.55	0.41
Yield of C ₂ H ₂	wt. %	83.01	83.50	68.65	66.78	39.10	70.00	16.50	20.00	8.50
SEC	kWh/kg C ₂ H ₂	13.73	14.57	21.40	21.13	42.62	18.00	88.58	144.43	258.51

4. Conclusion

In this work, the hydrolysis of liquid hydrocarbons including *n*-hexane and toluene in a rotating-arc plasma was investigated for the first time. The results verify that the rotating-arc plasma reactor shows lower SEC for the pyrolysis of liquid hydrocarbons than conventional plasma reactors, owing to the intensified mixing of reactants with hot plasma gas and more uniform temperature distribution. A lower H/C mole ratio of input materials could result in lower yield of C₂H₂ and lower SEC. With the increase in the energy input at the beginning, the C₂H₂ yield show a growing trend. However, excessive energy input is negative for the C₂H₂ yield due to the increasing C₂H₂ degradation rate. In the view of C₂H₂ yield and SEC, the optimum power input for *n*-hexane and toluene were 13.6 and 16.4 kW, respectively. The magnetic induction has slight effect on the pyrolysis of *n*-hexane. However, due to the stronger soot formation tendency, the pyrolysis of toluene performance was greatly affected by the magnetic induction, and the optimum magnetic induction range was 0.058–0.077 T. The pyrolysis of *n*-hexane to produce C₂H₂ is more efficient than the pyrolysis of toluene. Under the investigated conditions in this work, the maximum yield of C₂H₂ in the *n*-hexane pyrolysis could reach as high as 83.0% with the SEC of 13.7 kWh/kg·C₂H₂, and the maximum yield of C₂H₂ in the toluene pyrolysis could reach 68.6% with the SEC of 19.9 kWh/kg·C₂H₂. Overall, these results not only create new opportunity to improve the utilization of liquid hydrocarbons, but will also benefit the pyrolysis of other feedstock such as coal, coal tar and heavy oil in consideration of the advantages of rotating-arc plasma reactor.

Acknowledgments: This work was supported by the National Key Research and Development Program of China (2016YFB0301800) and the National High Technology Research and Development Program of China (2015AA020201).

Author Contributions: Qiwei Yang and Baogen Su conceived and designed the experiments; Ming Zhang, Jianhua Wu and Jie Ma performed the experiments; Guangdong Wen and Qilong Ren analyzed the data; Jie Ma wrote the paper.

Conflicts of Interest: The authors declare no conflict of interest.

Nomenclature

<i>B</i>	Magnetic induction (T)
<i>I</i>	Arc current (A)
<i>m</i>	Mass flow rate (g/min)
<i>P</i>	Power input (kW)
<i>Q</i>	Flow rate (Nm ³ /h)
BDE	Bond dissociation energy (kJ/mol)
PFR	Plug flow reactor
SEC	Specific energy consumption (kWh/kg C ₂ H ₂)

References

1. Lee, D.H.; Kim, K.T.; Song, Y.H.; Kang, W.S.; Jo, S. Mapping Plasma Chemistry in Hydrocarbon Fuel Processing Processes. *Plasma Chem. Plasma Process.* **2013**, *33*, 249–269. [[CrossRef](#)]
2. Fincke, J.R.; Anderson, R.P.; Hyde, T.; Detering, B.A.; Wright, R.; Bewley, R.L.; Haggard, D.C.; Swank, W.D. Plasma thermal conversion of methane to acetylene. *Plasma Chem. Plasma Process.* **2002**, *22*, 105–136. [[CrossRef](#)]
3. Dors, M.; Nowakowska, H.; Jasiński, M.; Mizeraczyk, J. Chemical Kinetics of Methane Pyrolysis in Microwave Plasma at Atmospheric Pressure. *Plasma Chem. Plasma Process.* **2014**, *34*, 313–326. [[CrossRef](#)]
4. Bidgoli, A.M.; Ghorbanzadeh, A.; Lotfalipour, R.; Roustaei, E.; Zakavi, M. Gliding spark plasma: Physical principles and performance in direct pyrolysis of methane. *Energy* **2017**, *125*, 705–715. [[CrossRef](#)]
5. Taghvaei, H.; Jahanmiri, A.; Rahimpour, M.R.; Shirazi, M.M.; Hooshmand, N. Hydrogen production through plasma cracking of hydrocarbons: Effect of carrier gas and hydrocarbon type. *Chem. Eng. J.* **2013**, *226*, 384–392. [[CrossRef](#)]

6. Yan, B.; Xu, P.; Li, X.; Guo, C.Y.; Jin, Y.; Cheng, Y. Experimental Study of Liquid Hydrocarbons Pyrolysis to Acetylene in H₂/Ar Plasma. *Plasma Chem. Plasma Process.* **2012**, *32*, 1203–1214. [[CrossRef](#)]
7. Yan, B.; Xu, P.; Guo, C.Y.; Jin, Y.; Cheng, Y. Experimental study on coal pyrolysis to acetylene in thermal plasma reactors. *Chem. Eng. J.* **2012**, *207*, 109–116. [[CrossRef](#)]
8. Messerle, V.E.; Ustimenko, A.B.; Lavrichshev, O.A. Comparative study of coal plasma gasification: Simulation and experiment. *Fuel* **2016**, *164*, 172–179. [[CrossRef](#)]
9. Cho, I.J.; Park, H.W.; Park, D.W.; Choi, S. Enhancement of synthesis gas production using gasification-plasma hybrid system. *Int. J. Hydrog. Energy* **2015**, *40*, 1709–1716. [[CrossRef](#)]
10. Mohsenian, S.; Esmaili, M.S.; Fathi, J.; Shokri, B. Hydrogen and carbon black nano-spheres production via thermal plasma pyrolysis of polymers. *Int. J. Hydrog. Energy* **2016**, *41*, 16656–16663. [[CrossRef](#)]
11. Marias, F.; Demarthon, R.; Bloas, A.; Robert-Arnouil, J.P.; Nebbad, F. Design of a High Temperature Reactor Fed by a Plasma Torch for Tar Conversion: Comparison between CFD Modelling and Experimental Results. *Waste Biomass Valoriz.* **2015**, *6*, 1–12. [[CrossRef](#)]
12. Zhang, M.; Xue, W.; Su, B.; Bao, Z.; Wen, G.; Xing, H.; Ren, Q. Conversion of glycerol into syngas by rotating DC arc plasma. *Energy* **2017**, *123*, 1–8. [[CrossRef](#)]
13. Zhang, Q.; Dor, L.; Zhang, L.; Yang, W.; Blasiak, W. Performance analysis of municipal solid waste gasification with steam in a Plasma Gasification Melting reactor. *Appl. Energy* **2012**, *98*, 219–229. [[CrossRef](#)]
14. Fabry, F.; Rehmet, C.; Rohani, V.; Fulcheri, L. Waste Gasification by Thermal Plasma: A Review. *Waste Biomass Valoriz.* **2013**, *4*, 421–439. [[CrossRef](#)]
15. Petitpas, G.; Rollier, J.D.; Darmon, A.; Gonzalez-Aguilar, J.; Metkemeijer, R.; Fulcheri, L. A comparative study of non-thermal plasma assisted reforming technologies. *Int. J. Hydrog. Energy* **2007**, *32*, 2848–2867. [[CrossRef](#)]
16. El-Tayeb, A.; El-Shazly, A.H.; Elkady, M.F. Investigation the Influence of Different Salts on the Degradation of Organic Dyes Using Non-Thermal Plasma. *Energies* **2016**, *9*, 874. [[CrossRef](#)]
17. Samal, S. Thermal plasma technology: The prospective future in material processing. *J. Clean. Prod.* **2017**, *142*, 3131–3150. [[CrossRef](#)]
18. Mostaghimi, J.; Boulos, M.I. Thermal Plasma Sources: How Well are They Adopted to Process Needs? *Plasma Chem. Plasma Process.* **2015**, *35*, 421–436. [[CrossRef](#)]
19. Tamošiūnas, A.; Chouchène, A.; Valatkevičius, P.; Gimžauskaitė, D.; Aikas, M.; Uscila, R.; Ghorbel, M.; Jeguirim, M. The Potential of Thermal Plasma Gasification of Olive Pomace Charcoal. *Energies* **2017**, *10*, 710. [[CrossRef](#)]
20. Gabbar, H.A.; Aboughaly, M.; Stoute, C.A. DC Thermal Plasma Design and Utilization for the Low Density Polyethylene to Diesel Oil Pyrolysis Reaction. *Energies* **2017**, *10*, 784. [[CrossRef](#)]
21. Schobert, H. Production of Acetylene and Acetylene-based Chemicals from Coal. *Chem. Rev.* **2014**, *114*, 1743–1760. [[CrossRef](#)] [[PubMed](#)]
22. Su, C.; Wang, D.; Wang, T. Simulation of partial oxidation of natural gas with detailed chemistry: Influence of addition of H₂, C₂H₆ and C₃H₈. *Chem. Eng. Sci.* **2010**, *65*, 2608–2618.
23. Mosse, A.L.; Gorbunov, A.V.; Galinovskii, A.A.; Savchin, V.V.; Lozhechnik, A.V. Production of commercial hydrogen and acetylene from propane-butane and liquid hydrocarbons in an electric-arc plasma reactor. *J. Eng. Phys. Thermophys.* **2008**, *81*, 652–658. [[CrossRef](#)]
24. Zhang, M.; Ma, J.; Su, B.; Wen, G.; Yang, Q.; Ren, Q. Pyrolysis of Polyolefins Using Rotating Arc Plasma Technology for Production of Acetylene. *Energies* **2017**, *10*, 513. [[CrossRef](#)]
25. Wang, S.; Chen, H.G.; Xie, K.C. The effect of component of coal on the yield of acetylene in arc plasma pyrolysis. *Chem. Ind. Eng.* **2003**, *20*, 195–199. (In Chinese)
26. Beiers, H.G.; Baumann, H.; Bittner, D.; Klein, J.; Jüntgen, H. Pyrolysis of some gaseous and liquid hydrocarbons in hydrogen plasma. *Fuel* **1988**, *67*, 1012–1016. [[CrossRef](#)]
27. Pfender, E. Thermal Plasma Technology: Where Do We Stand and Where Are We Going? *Plasma Chem. Plasma Process.* **1999**, *19*, 1–31. [[CrossRef](#)]
28. Wu, A.; Li, X.; Chen, L.; Zhu, F.; Zhang, H.; Du, C.; Yan, J. Utilization of waste rapeseed oil by rotating gliding arc plasma. *Int. J. Hydrog. Energy* **2015**, *40*, 9039–9048. [[CrossRef](#)]
29. Ma, J.; Zhang, M.; Su, B.; Wen, G.; Yang, Y.; Yang, Q.; Ren, Q. Numerical simulation of the entrained flow hydrolysis of coal in magnetically rotating plasma reactor. *Energy Convers. Manage.* **2017**, *148*, 431–439. [[CrossRef](#)]

30. Ma, J.; Wen, G.D.; Su, B.G.; Yang, Y.W.; Ren, Q.L. Current-voltage characteristics of hydrogen DC plasma torches with different sizes in an external axial magnetic field. *Chinese Phys. B* **2015**, *24*, 65205. [CrossRef]
31. Ma, J.; Su, B.; Wen, G.; Ren, Q.; Yang, Y.; Yang, Q.; Xing, H. Kinetic modeling and experimental validation of the pyrolysis of propane in hydrogen plasma. *Int. J. Hydrog. Energy* **2016**, *41*, 22689–22697. [CrossRef]
32. Demidov, D.V.; Mishin, I.V.; Mikhailov, M.N. Gibbs free energy minimization as a way to optimize the combined steam and carbon dioxide reforming of methane. *Int. J. Hydrog. Energy* **2011**, *36*, 5941–5950. [CrossRef]
33. Wang, H.; Dames, E.; Sirjean, B.; Sheen, D.A.; Tango, R.; Violi, A.; Lai, J.Y.W.; Egolfopoulos, F.N.; Davidson, D.F.; Hanson, R.K.; et al. high-temperature chemical kinetic model of n-alkane (up to n-dodecane), cyclohexane, and methyl-, ethyl-, n-propyl and n-butyl-cyclohexane oxidation at high temperatures, JetSurF version 2.0. Available online: <http://web.stanford.edu/group/haiwanglab/JetSurF/JetSurF2.0/index.html> (accessed on 19 September 2010).
34. Wang, H.; You, X.; Joshi, A.V.; Davis, S.G.; Laskin, A.; Egolfopoulos, F.; Law, C.K. High-Temperature Combustion Reaction Model of H₂/CO/C₁–C₄ Compounds, USC Mech Version II. Available online: http://ignis.usc.edu/Mechanisms/USC-Mech%20II/USC_Mech%20II.htm (accessed on 1 May 2007).
35. Zhang, L.; Cai, J.; Zhang, T.; Qi, F. Kinetic modeling study of toluene pyrolysis at low pressure. *Combust. Flame* **2010**, *157*, 1686–1697. [CrossRef]
36. Huang, X.; Cheng, D.G.; Chen, F.; Zhan, X. The decomposition of aromatic hydrocarbons during coal pyrolysis in hydrogen plasma: A density functional theory study. *Int. J. Hydrog. Energy* **2012**, *37*, 18040–18049. [CrossRef]
37. Huang, X.; Cheng, D.; Chen, F.; Zhan, X. A density functional theory study on the decomposition of aliphatic hydrocarbons and cycloalkanes during coal pyrolysis in hydrogen plasma. *J. Energy Chem.* **2015**, *24*, 65–71. [CrossRef]
38. Richter, H.; Howard, J.B. Formation of polycyclic aromatic hydrocarbons and their growth to soot—A review of chemical reaction pathways. *Prog. Energy Combust.* **2000**, *26*, 565–608. [CrossRef]
39. Agafonov, G.L.; Biler, I.V.; Vlasov, P.A.; Zhil'tsova, I.V.; Kolbanovskii, Y.A.; Smirnov, V.N.; Tereza, A.M. Unified kinetic model of soot formation in the pyrolysis and oxidation of aliphatic and aromatic hydrocarbons in shock waves. *Kinet. Catal.* **2016**, *57*, 557–572. [CrossRef]
40. Luo, Y. *Handbook of Bond Dissociation Energies in Organic Compounds*; CRC press: Boca Raton, FL, USA, 2002.
41. Richter, H.; Granata, S.; Green, W.H.; Howard, J.B. Detailed modeling of PAH and soot formation in a laminar premixed benzene/oxygen/argon low-pressure flame. *Proc. Combust. Inst.* **2005**, *30*, 1397–1405. [CrossRef]
42. Essiptchouk, A.M.; Sharakhovsky, L.I.; Marotta, A. A new formula for the rotational velocity of magnetically driven arcs. *J. Phy. D: Appl. Phy.* **2000**, *33*, 2591. [CrossRef]



© 2017 by the authors. Licensee MDPI, Basel, Switzerland. This article is an open access article distributed under the terms and conditions of the Creative Commons Attribution (CC BY) license (<http://creativecommons.org/licenses/by/4.0/>).